JACS
JOURNAL OF THE AMERICAN CHEMICAL SOCIETY

Communication

pubs.acs.org/JACS

General Space-Confined On-Substrate Fabrication of Thickness-Adjustable Hybrid Perovskite Single-Crystalline Thin Films

Yao-Xuan Chen,[†,‡,§] Qian-Qing Ge,[†,‡,§] Yang Shi,[†,‡] Jie Liu,[†,‡] Ding-Jiang Xue,[†,‡] Jing-Yuan Ma,[†,‡] Jie Ding,[†,‡] Hui-Juan Yan,[†,‡] Jin-Song Hu,*[,†,‡] and Li-Jun Wan*[,†,‡]

[†]Key Laboratory of Molecular Nanostructure and Nanotechnology, Institute of Chemistry, Chinese Academy of Science, 2 North 1st Street, Zhongguancun, Beijing 100190, China

[‡]University of Chinese Academy of Science, Beijing 100049, China

Supporting Information

ABSTRACT: Organic−inorganic hybrid perovskite single-crystalline thin films (SCTFs) are promising for enhancing photoelectric device performance due to high carrier mobility, long diffusion length, and carrier lifetime. However, bulk perovskite single crystals available today are not suitable for practical device application due to the unfavorable thickness. Herein, we report a facile space-confined solution-processed strategy to on-substrate grow various hybrid perovskite SCTFs in a size of submillimeter with adjustable thicknesses from nano- to micrometers. These SCTFs exhibit photoelectric properties comparable to bulk single crystals with low defect density and good air stability. The clear thickness-dependent colors allow fast visual selection of SCTFs with a suitable thickness for specific device application. The present substrate-independent growth of perovskite SCTFs opens up opportunities for on-chip fabrication of diverse high-performance devices.

Organic−inorganic hybrid perovskites have been demonstrated in many optoelectronic applications including high-efficiency perovskite solar cells (PSCs),[1−4] solid-state lasers,[5] light-emitting diodes,[6] and highly sensitive photodetectors,[7,8] due to their superior photoelectric properties such as high absorption coefficient, long carrier lifetime, and highly balanced hole and electron mobility.[9] Although the hybrid perovskites have been extensively studied, it is worth noting that the perovskite absorber layers in PSCs, even the best one reached a certified 22.1% power conversion efficiency (PCE),[10,11] are based on microcrystallines.[12] This could be limited by the lack of a facile and effective way to fabricate large single-crystalline thin films. Bulk perovskite single crystals show significantly higher carrier mobility and longer diffusion length and carrier lifetime due to the reduced trap-state densities by orders of magnitude compared with polycrystalline films. These attractive improvements stem from the considerable removal of grain boundaries (GBs).[13−15] Moreover, the broader light-absorption of perovskite single crystal significantly increases the theoretic current density,[13,15] resulting in a higher PCE in PSCs or a broader working range in photodetectors. With these improved properties, the single-crystalline perovskites have promising potential in photoelectric devices.

In the PSC field, much effort and great progress has been made by improving the growth of perovskite grains. Perovskite films with grain sizes up to several micrometers have been achieved, thus significantly enhancing PCEs of PSCs by increasing open circuit voltage (V_{OC}) and fill factor (FF) due to the notable elimination of GBs and thus carrier recombination. However, application of current bulk single crystals in device fabrication may cause degradation of device performance due to the increase of charge recombination as active layer thickness increases. Toward this end, the fabrication of perovskite single-crystalline thin films (SCTFs) is highly desirable and intriguing to boost device performance.[16−19] Unfortunately, the current methods tend to grow thicker bulk single crystals with small aspect ratios,[13−15,20] which needs further processing for practical device applications. Herein, we report controllable fabrication of submillimeter-size, air-stable perovskite SCTFs. The thickness of SCTFs can be adjusted from nano- to micrometers with an aspect ratio up to ~10^5. The strategy enables on-substrate growth of various perovskite SCTFs. The substrate-independent growth and thickness-dependent colors of SCTFs are intriguing for the direct fabrication and visual selection SCTFs with suitable thickness for diverse devices.

As depicted in Figure 1, two clean flat substrates were clipped together and then vertically dipped in perovskite precursor

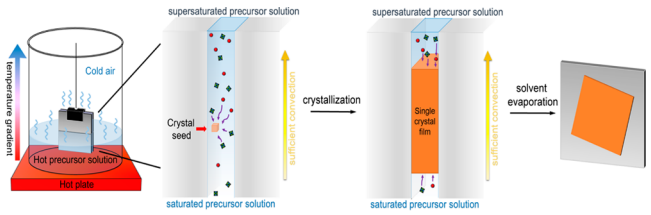

Figure 1. (a) Scheme for growth of perovskite SCTFs.

solution. The capillary pressure drove the solution onto the whole substrates. The thickness of solution film depended on the distance between substrates, which can be easily tuned from nano- to micrometers by clipping force. Subsequently, the bottom precursor solution was heated to control the evaporation rate of solvent. Following top-seeded solution-growth (TSSG),[13] the bottom solution maintained saturated conditions and the top

Received: September 6, 2016
Published: November 27, 2016

DOI: 10.1021/jacs.6b09388
J. Am. Chem. Soc. 2016, 138, 16196−16199

solution film was supersaturated due to the cooler condition, inducing the crystallization of perovskite in the clipped solution film. Simultaneously, a temperature gradient caused sufficient convection from bottom to top, supplying the material for the continuous growth of perovskite single crystals. After a certain time, perovskite SCTFs would form in the confined space by the clipped substrates. The thickness of SCTFs was well-defined by the distance between two substrates, which can be easily tuned by clipping force.

The influence of solvents on the growth of SCTFs was first investigated because the solubility of perovskite precursors MAX ($MA = CH_3NH_3^+$) and PbX_2 (X = I, Br, Cl) and the volatilization rate of solvent affected the TSSG process. It was found that three common solvents of γ-butyrolactone (GBA), *N*,*N*-dimethylformamide (DMF), and dimethyl sulfoxide (DMSO) with balanced solubility and volatilization rates were suitable for the growth of $MAPbI_3$, $MAPbBr_3$, and $MAPbCl_3$, respectively.[13,15,20] Second, we tested the influence of substrates. It was found that the perovskite SCTF growth did not require lattice match with the substrate. It could be directly grown on a variety of flat substrates including silicon wafer (with or without dielectric film), flexible plastic substrate such as polyethylene terephthalate (PET), glass, quartz, mica, ITO, FTO, HOPG, etc. This substrate-independent growth brought appealing potentials to on-chip fabricate perovskite devices for diverse applications, e.g., SCTF/ITO for PSCs, SCTF/quartz for optical devices, SCTF/Si for electronic devices, SCTF/PET for flexible devices, etc. Figure S1 representatively presented the typical scanning electron microscopy (SEM) and optical images of $MAPbBr_3$ SCTFs on different substrates. A typical SEM image of $MAPbBr_3$ SCTF grown on ITO/glass and the corresponding energy dispersive spectroscopy (EDS) mapping images proofed that the $MAPbBr_3$ film could be grown on ITO (Figure S2). To test the physical contact of SCTFs, the SCTFs on silicon, PET, and ITO/glass were ultrasonically treated in chlorobenzene at power of 500 W and visually inspected with a microscope. After 10 min ultrasonic treatment, no visible peeling off or move was observed.

Taking various perovskite SCTFs grown on PET as examples, SEM (Figure 2a) and optical microscopy (Figure S1d) showed that a flat thin film with a regular shape and a size of hundreds of micrometers was obtained. A zoom-in SEM image (Figure 2b) clearly disclosed the angled facets and smooth surfaces without visible grain boundaries and voids. Even in high-resolution SEM images, no grain structure was observed on three types of SCTFs, further evidencing their single-crystalline nature (Figure S3). Such SCTFs up to millimeter size could be observed during the SEM observation. $MAPbCl_3$ and $MAPbI_3$ SCTFs displayed flat GB-free crystalline morphologies similar to $MAPbBr_3$, as seen in SEM images (Figure 2c,d) and optical microscopy images (Figure S1e,f). The composition of these perovskite SCTFs were confirmed by the EDS analysis (Figure S4). The EDS mapping images indicated the uniform distribution of N, Pb, and halogens with a near theoretical composition ratio. It was noted the shapes of perovskite SCTFs were related to their crystallographic system to some extent. The more regularly shaped SCTFs were observed on cubic $MAPbBr_3$ and $MAPbCl_3$ whereas tetragonal $MAPbI_3$ usually gave a little larger SCTFs under the same growth condition. Different from cubic $MAPbCl_3$ and $MAPbBr_3$ SCTFs with well-defined right angular edges, the tetragonal $MAPbI_3$ films usually showed the edges with oblique angles (Figure S5).

The thickness of perovskite film is critical for practical photoelectric device applications because it significantly affects light harvest and carrier recombination. We found the thickness of the prepared perovskite SCTF could be easily adjusted by the distance between the clipped substrates. This distance defined the thickness of the clipped precursor solution film, which supplied raw materials MAX and PbX_2 for the formation of perovskite and limited its growth in the direction perpendicular to substrate. Consequently, we could tune the thickness of SCTFs by controlling the applied pressure on substrates.

Atomic force microscopy (AFM) profiles and 3D images (Figure 3a,b) revealed the successful fabrication of $MAPbBr_3$ SCTFs in a thickness ranging from a few nanometers to micrometers, which was much less than the film size and very suitable for the light absorption layer of PSCs and photodetectors.[21,22] Figure 3c depicted the relationship between the

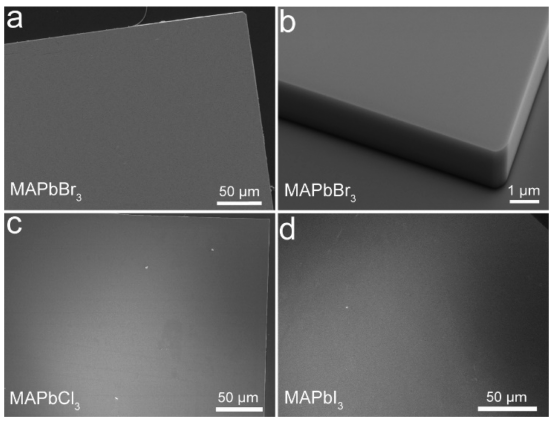

Figure 2. (a,b) SEM images of $MAPbBr_3$ SCTFs grown on PET: (a) Top view and (b) 70° rotation view. (c,d) Top-view SEM images of (c) $MAPbCl_3$ and (d) $MAPbI_3$ SCTFs grown on PET.

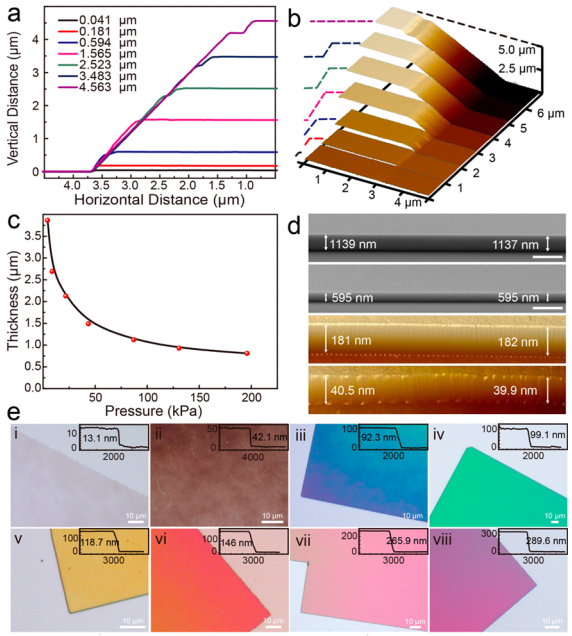

Figure 3. (a) AFM sectional profiles and (b) 3D images of $MAPbBr_3$ SCTF with various thickness. (c) Nonlinear correlation of SCTF thickness and applied pressure. (d) Cross section SEM images and AFM images of $MAPbBr_3$ SCTFs with varied thicknesses. Scale bar in SEM images is 2 μm. (e) Optical images of ultrathin $MAPbBr_3$ SCTFs showing the thickness-dependent colors.

DOI: 10.1021/jacs.6b09388
J. Am. Chem. Soc. 2016, 138, 16196−16199

applied pressures and average thicknesses of SCTFs. It showed a clear tendency that the thicknesses of SCTFs were nonlinearly inversely proportional to the applied pressures. For example, when the pressure increased from 10 to 25 kPa, the average thickness of SCTF decreased from 2.8 to 2.0 μm. The further increase of pressure to 200 kPa achieved a thickness of 0.8 μm. If the pressure was too low, it would be difficult to confine stably the precursor solution film, leading to plenty of micrometer-size crystalline grains. Through increasing the force applied on the substrates, ultrathin perovskite SCTFs with a thicknesses down to hundreds of and even tens of nanometers could be obtained. Cross section SEM or AFM images (Figure 3d) evidenced the thicknesses of perovskite SCTFs were uniform, as indicated by the flat plateaus in AFM profiles (Figure 3a).

Moreover, perovskite SCTFs with different thicknesses in nanometer range exhibited characteristic colors in optical observation (Figure 3e). This phenomenon was due to the effect of thin film interference. When the actual optical path in perovskite SCTF was an integral multiple of light wavelength: $2n_1d = k\lambda(k = 1,2,3...)$, where n_1, d, and λ are refractive index, SCTF thickness, and light wavelength, respectively, the reflected light would be enhanced so that we saw the color of enhanced light. This facile direct visual inspection allowed us to harvest quickly the SCTFs with a certain thickness to meet diverse practical needs.

X-ray diffraction with a 2D detector is a technique to determine whether a film is single crystalline. The crystalline structure of $MAPbBr_3$ SCTF on PET substrate was probed using synchrotron X-ray radiation and a 2D detector. As shown in Figure 4a, only one set of well-defined diffraction matrix was collected during the ±5° rotation of radiation beam angle, which could be well-indexed to the diffractions from cubic phase perovskite. All diffuse diffraction rings were from PET substrate by comparison with the pattern collected on blank PET film (Figure S6). This result suggested the measured $MAPbBr_3$ film should be single crystalline. To probe further the growth orientation of $MAPbBr_3$ SCTF, a still-mode synchrotron X-ray diffraction image in perpendicular incidence was also collected (Figure 4b). After subtraction of the PET background, a bright diffraction spot indexed to the diffraction from (100) planes was detected. Together with the result in Figure 4a, this result indicated that the in-plane orientation of the film was (100) planes. This still-mode image was further integrated and compared with the conventional XRD pattern of $MAPbBr_3$ powder crushed from a single crystal (Figure 4c). After the calibration of the monochromatic synchrotron beam to Cu Kα, the bright spot on the still-mode synchrotron diffraction image (Figure 4b) corresponded to the diffraction peak (pattern iv, Figure 4c), which matched well with the position of (100) crystallographic planes. A similar synchrotron X-ray diffraction image and the corresponding XRD pattern were observed on the $MAPbBr_3$ SCTF/glass substrate (Figure S7). Furthermore, the XRD pattern of $MAPbBr_3$ powder crushed from the prepared single crystal displayed the typical cubic crystalline structure of perovskite $MAPbBr_3$ (Figure 4c), similar to that of $MAPbBr_3$ film for PSC applications.[23] Compared with XRD patterns of the starting materials (Figure 4c), there was no diffraction from these possible impurities. Moreover, after 5 months of exposure to ambient air with 20% RH at room temperature, there was no change observed for the XRD pattern of $MAPbBr_3$ SCTF (Figure S8), indicating its excellent air stability. EBSD is a powerful technique to inspect phase purity and the quality of crystalline materials by offering electron diffraction information in hundred micrometers scale regardless of thickness. As shown in Figure 4d, the EBSD image of $MAPbBr_3$ SCTF gave uniform color over the entire film, revealing its pure crystalline phase and high crystalline quality. In short, the above results conclude a high-quality, phase-pure single-crystalline $MAPbBr_3$ thin film with excellent long-term stability can be obtained by the present method.

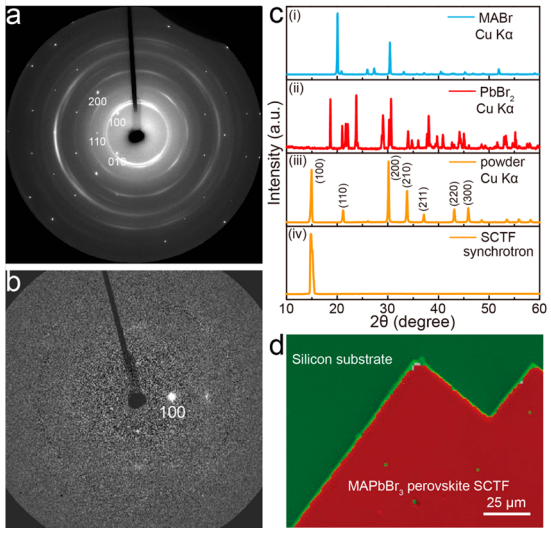

Figure 4. (a,b) Synchrotron X-ray diffraction images of $MAPbBr_3$ SCTF on PET substrate collected with a 2D detector: (a) by rotating incident radiation of ±5°. All diffuse diffraction rings can be attributed to PET substrate. (b) Still-mode image in perpendicular incidence after the subtraction of PET background. (c) XRD patterns recorded using Cu Kα radiation: (i) MABr powder, (ii) $PbBr_2$ powder, and (iii) $MAPbBr_3$ powder ground from a single crystal. (iv) XRD pattern integrated from panel b after the calibration to Cu Kα. (d) EBSD phase image of $MAPbBr_3$ SCTF grown on silicon substrate.

The optical properties of perovskite SCTFs were investigated using photoluminescence (PL) and steady-state absorption spectroscopy. As shown in Figure 5a, $MAPbBr_3$ SCTF showed absorption starting from ~550 nm, corresponding to its orange color. The clear band edge cutoff with no excitonic signature or absorption tails was characteristic of high-quality crystals with a low concentration of in-gap defects.[15] The narrow PL peak at

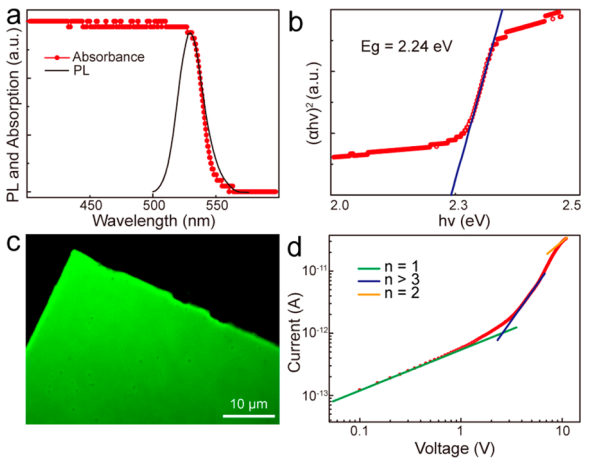

Figure 5. (a) PL and steady-state absorption spectra, (b) optical bandgap, (c) confocal laser scanning microscopy image, and (d) typical dark $I-V$ trace of $MAPbBr_3$ SCTF.

DOI: 10.1021/jacs.6b09388
J. Am. Chem. Soc. 2016, 138, 16196−16199

~530 nm was shorter than the absorption onsets, implying the PL emission could be extinguished by themselves, consistent with the result of bulk single crystals.[13] The optical bandgap of $MAPbBr_3$ SCTF was extracted to be 2.24 eV (Figure 5b),[15] consistent with previously reported values for bulk single crystal and planar-integrated single crystalline film.[15,17] Similarly, the analyses on the absorption spectra of $MAPbCl_3$ and $MAPbI_3$ SCTFs gave their optical bandgap of 3.0 and 1.53 eV, respectively (Figure S9). Moreover, the confocal laser scanning microscopy image (Figure 5c) of $MAPbBr_3$ SCTF showed bright and uniform luminescence, corroborating its high quality without visible defects.

The space charge limited current method was used to investigate transport properties of $MAPbBr_3$ SCTF. The device dark $I-V$ curve was measured to derive trap density and carrier mobility (μ).[13] As shown in Figure 5d, the linear $I-V$ section at the low voltage was an ohmic region (green). As the $I-V$ curve went to a higher bias, it followed by a steep increase, indicating the presence of a trap-filling region (blue) starting at trap-filled limit voltage (V_{TFL}). The n_{trap} calculated from V_{TFL} was 4.8×10^{10} cm^{-3} (Supporting Information), comparable to bulk single crystal and several orders of magnitude lower than polycrystalline films.[13−15,17,20] When the applied voltage kept going to the Child's regime (orange), the μ was deduced to be 15.7 $cm^2\ V^{-1}\ s^{-1}$ by fitting the curve with the Mott−Gurney law (Supporting Information).[20,22] To evaluate the optoelectronic quality of the prepared perovskite films, the carrier lifetime (τ_r) of $MAPbI_3$ SCTF was measured by impedance spectroscopy (Figure S10).[13] The τ_r of 84 μs was close to that of the bulk $MAPbI_3$ single crystal (98 μs), indicating the comparable optoelectronic quality.

In summary, a general facile strategy was successfully developed to on-substrate fabricate large-area single-crystalline hybrid perovskite thin films with tunable thickness. The prepared perovskite SCTFs exhibited excellent air stability and comparable quality to bulk single crystals with an n_{trap} of 4.8×10^{10} cm^{-3}, μ of 15.7 $cm^2\ V^{-1}\ s^{-1}$, and τ_r of 84 μs. These results might inspire further exploration of on-chip fabrication of high-performance PSCs and diverse devices with hybrid perovskite SCTFs.

■ ASSOCIATED CONTENT

Supporting Information

The Supporting Information is available free of charge on the ACS Publications website at DOI: 10.1021/jacs.6b09388.

Experimental section (PDF)

■ AUTHOR INFORMATION

Corresponding Authors

*J.-S.H. hujs@iccas.ac.cn

*L.-J.W. wanlijun@iccas.ac.cn

ORCID

Jin-Song Hu: 0000-0002-6268-0959

Author Contributions

§These authors contributed equally.

Notes

The authors declare no competing financial interest.

■ ACKNOWLEDGMENTS

The financial supports are from the National Key Project on Basic Research (2015CB932302), the National Natural Science Foundation of China (21573249), and the Strategic Priority Research Program of the Chinese Academy of Sciences (Grant No. XDB12020100). We thank A. G. Li, Z. H. Dong, S. Jiang, and L. L. Zhang at the BL15U1 at Shanghai Synchrotron Radiation Facility; J. Q. Zhang and Z. X. Wei at National Center for Nanoscience and Technology; G. J. Song at ICCAS; and S. F. Jin at Institute of Physics, CAS for their help on XRD analyses.

■ REFERENCES

(1) Lee, M.; Teuscher, J.; Miyasaka, T.; Murakami, T. N.; Snaith, H. J. *Science* **2012**, *338*, 643−647.

(2) Jeon, N. J.; Lee, H. G.; Kim, Y. C.; Seo, J.; Noh, J. H.; Lee, J.; Seok, S. I. *J. Am. Chem. Soc.* **2014**, *136*, 7837−7840.

(3) Zhou, H.; Chen, Q.; Li, G.; Luo, S.; Song, T.-b.; Duan, H.-S.; Hong, Z.; You, J.; Liu, Y.; Yang, Y. *Science* **2014**, *345*, 542−546.

(4) Jeon, N. J.; Noh, J. H.; Yang, W. S.; Kim, Y. C.; Ryu, S.; Seo, J.; Seok, S. I. *Nature* **2015**, *517*, 476−480.

(5) Xing, G.; Mathews, N.; Lim, S. S.; Yantara, N.; Liu, X.; Sabba, D.; Grätzel, M.; Mhaisalkar, S.; Sum, T. C. *Nat. Mater.* **2014**, *13*, 476−480.

(6) Tan, Z.-K.; Moghaddam, R.; Lai, M.; Docampo, P.; Higler, R.; Deschler, F.; Price, M.; Sadhanala, A.; Pazos, L. M.; Credgington, D.; Hanusch, F.; Bein, T.; Snaith, H. J.; Friend, R. H. *Nat. Nanotechnol.* **2014**, *9*, 687−692.

(7) Dou, L.; Yang, Y. M.; You, J.; Hong, Z.; Chang, W.-H.; Li, G.; Yang, Y. *Nat. Commun.* **2014**, *5*, 5404.

(8) Fang, Y.; Dong, Q.; Shao, Y.; Yuan, Y.; Huang, J. *Nat. Photonics* **2015**, *9*, 679−686.

(9) Xing, G.; Mathews, N.; Sun, S.; Lim, S. S.; Lam, Y. M.; Grätzel, M.; Mhaisalkar, S.; Sum, T. C. *Science* **2013**, *342*, 344−347.

(10) http://www.nrel.gov/ncpv/images/efficiency_chart.jpg.

(11) Saliba, M.; Matsui, T.; Seo, J.-Y.; Domanski, K.; Correa-Baena, J.-P.; Nazeeruddin, M.; Zakeeruddin, S. M.; Tress, W.; Abate, A.; Hagfeldt, A.; Grätzel, M. *Energy Environ. Sci.* **2016**, *9*, 1989−1997.

(12) Stranks, S. D.; Eperon, G. E.; Grancini, G.; Menelaou, C.; Alcocer, M. J.; Leijtens, T.; Herz, L. M.; Petrozza, A.; Snaith, H. J. *Science* **2013**, *342*, 341−344.

(13) Dong, Q.; Fang, Y.; Shao, Y.; Mulligan, P.; Qiu, J.; Cao, L.; Huang, J. *Science* **2015**, *347*, 967−970.

(14) Shi, D.; Adinolfi, V.; Comin, R.; Yuan, M.; Alarousu, E.; Buin, A.; Chen, Y.; Hoogland, S.; Rothenberger, A.; Katsiev, K.; Losovyj, Y.; Zhang, X.; Dowben, P. A.; Mohammed, O. F.; Sargent, E. H.; Bakr, O. M. *Science* **2015**, *347*, 519−522.

(15) Liu, Y.; Yang, Z.; Cui, D.; Ren, X.; Sun, J.; Liu, X.; Zhang, J.; Wei, Q.; Fan, H.; Yu, F.; Zhang, X.; Zhao, C.; Liu, S. *Adv. Mater.* **2015**, *27*, 5176−5183.

(16) Dou, L.; Wong, A. B.; Yu, Y.; Lai, M.; Kornienko, N.; Eaton, S. W.; Fu, A.; Bischak, C. G.; Ma, J.; Ding, T.; Ginsberg, N. S.; Wang, L.-W.; Alivisatos, A. P.; Yang, P. *Science* **2015**, *349*, 1518−1521.

(17) Saidaminov, M. I.; Adinolfi, V.; Comin, R.; Abdelhady, A. L.; Peng, W.; Dursun, I.; Yuan, M.; Hoogland, S.; Sargent, E. H.; Bakr, O. M. *Nat. Commun.* **2015**, *6*, 8724.

(18) Peng, W.; Wang, L.; Murali, B.; Ho, K.-T.; Bera, A.; Cho, N.; Kang, C.-F.; Burlakov, V. M.; Pan, J.; Sinatra, L.; Ma, C.; Xu, W.; Shi, D.; Alarousu, E.; Goriely, A.; He, J.-H.; Mohammed, O. F.; Wu, T.; Bakr, O. M. *Adv. Mater.* **2016**, *28*, 3383−3390.

(19) Liu, Y.; Zhang, Y.; Yang, Z.; Yang, D.; Ren, X.; Pang, L.; Liu, S. *Adv. Mater.* **2016**, *28*, 9204−9209.

(20) Saidaminov, M. I.; Abdelhady, A. L.; Murali, B.; Alarousu, E.; Burlakov, V. M.; Peng, W.; Dursun, I.; Wang, L.; He, Y.; Maculan, G.; Goriely, A.; Wu, T.; Mohammed, O. F.; Bakr, O. M. *Nat. Commun.* **2015**, *6*, 7586.

(21) Jung, H.; Park, N. G. *Small* **2015**, *11*, 10−25.

(22) Huang, J.; Shao, Y.; Dong, Q. *J. Phys. Chem. Lett.* **2015**, *6*, 3218−3227.

(23) Kim, Y.-H.; Cho, H.; Heo, J. H.; Kim, T.-S.; Myoung, N.; Lee, C.-L.; Im, S. H.; Lee, T.-W. *Adv. Mater.* **2015**, *27*, 1248−1254.

DOI: 10.1021/jacs.6b09388
J. Am. Chem. Soc. 2016, 138, 16196−16199